Electrochimica Acta 374 (2021) 137820

Contents lists available at ScienceDirect

Electrochimica Acta

journal homepage: www.elsevier.com/locate/electacta

Effect of pressure and temperature on carbon dioxide reduction at a plasmonically active silver cathode

Elizabeth R. Corson[a,b,*], Erin B. Creel[b,c,d,1], Robert Kostecki[b,e], Jeffrey J. Urban[b,c], Bryan D. McCloskey[a,b,e]

[a] Department of Chemical and Biomolecular Engineering, 201 Gilman Hall, University of California, Berkeley, CA 94720, USA
[b] Joint Center for Artificial Photosynthesis, Lawrence Berkeley National Laboratory, 1 Cyclotron Road, Building 30, Berkeley, CA 94720, USA
[c] The Molecular Foundry, Lawrence Berkeley National Laboratory, 1 Cyclotron Road, Building 67, Berkeley, CA 94720, USA
[d] Department of Chemistry, 419 Latimer Hall, University of California, Berkeley, CA 94720, USA
[e] Energy Storage and Distributed Resources Division, Lawrence Berkeley National Laboratory, 1 Cyclotron Road, Building 70, Berkeley, CA 94720, USA

ARTICLE INFO

Article history:
Received 27 September 2020
Revised 21 November 2020
Accepted 13 January 2021
Available online 29 January 2021

Keywords:
Carbon dioxide reduction
Plasmon-enhanced electrocatalysis
Silver film
Carbon dioxide partial pressure
Reaction order

ABSTRACT

Carbon dioxide (CO_2) reduction at a plasmonically active silver cathode was investigated by varying the pressure and temperature at multiple applied potentials under both dark and illuminated conditions to understand the mechanism of selectivity changes driven by plasmon-enhanced electrochemical conversion. CO_2 partial pressures (P_{CO_2}) from 0.2 to 1 atm were studied during linear sweep voltammetry and chronoamperometry at −0.7, −0.9, and −1.1 V_{RHE}. At a given applied overpotential the total current density increased with increasing P_{CO_2} in both the dark and the light, but there were significant differences in the Tafel behavior between dark and illuminated conditions. The reduction of CO_2 to carbon monoxide (CO) was found to have first-order behavior with respect to P_{CO_2} at all applied potentials in both the dark and the light, likely indicating no change in the rate-determining step upon illumination. Activity for the hydrogen (H_2) evolution reaction decreased with increasing P_{CO_2} at slightly different rates in the dark and the light at each applied potential, making it unclear if light is influencing CO or H_2 intermediate adsorbate coverage. Both formate and methanol production showed no dependence on P_{CO_2} under any conditions, but the true reaction orders may be masked by the much higher activity for CO and H_2 at the silver cathode. The investigation of product distribution with temperature at 14, 22, and 32°C at −0.7, −0.9, and −1.1 V_{RHE} in both the dark and the light demonstrated that the selectivity changes observed upon illumination are not caused by local heating of the cathode surface.

1. Introduction

Carbon dioxide (CO_2) can be electrochemically reduced to form valuable products such as renewable fuels and chemical precursors, preventing the need for CO_2 sequestration. The key challenge in CO_2 reduction is developing a catalyst that is highly selective to a single product at a low overpotential. Plasmon-enhanced electrochemical reduction of CO_2 has been shown to increase the selectivity and efficiency towards CO_2 reduction products while simultaneously suppressing hydrogen (H_2) evolution at both silver (Ag) and copper (Cu) cathodes [1–3]. While this is a promising field, we need to develop a better understanding of the plasmonic mechanisms that drive these selectivity changes to design more effective CO_2 reduction catalysts.

In previous work we showed that a plasmonically active Ag cathode selectively produced carbon monoxide (CO) and suppressed activity towards H_2 evolution upon illumination at low overpotentials (−0.6 to −0.8 V vs. the reversible hydrogen electrode (V_{RHE})) [2]. Formate production was enhanced in the light at potentials more negative than −0.7 V_{RHE} [2]. Methanol was formed upon illumination beginning at −0.8 V_{RHE} and reached a Faradaic efficiency (FE) of 2% at −1.1 V_{RHE}, representing a 550 mV decrease in the onset potential and a 100-fold increase in selectivity when compared to results on a Ag foil in the dark [2,4]. The exact plasmonic mechanisms that are responsible for these changes are still unknown.

Here we study CO_2 reduction at the same plasmonically active Ag cathode reported by Creel et al. [2] in the dark and the light at

* Corresponding author at: Department of Chemical Engineering, Stanford University, 443 Via Ortega, Stanford, CA 94305, USA.
E-mail addresses: ecorson@stanford.edu (E.R. Corson), bmcclosk@berkeley.edu (B.D. McCloskey).
[1] Present address: Electrification and Energy Infrastructures Division, Oak Ridge National Laboratory, 1 Bethel Valley Rd., Oak Ridge, TN 37830, USA.

https://doi.org/10.1016/j.electacta.2021.137820
0013-4686/

partial pressures of CO_2 (P_{CO_2}) from 0.2 to 1 atm and at electrolyte temperatures from 14 to 32°C across a range of applied potentials (−0.7, −0.9, and −1.1 V_{RHE}) to shed light on the plasmonic mechanisms directing the previously reported selectivity changes. We selected these three potentials to focus on the key findings of the previous study: CO was enhanced and H_2 suppressed at −0.7 V_{RHE}, the difference between formate production in the light compared to the dark was maximized at −0.9 V_{RHE}, and methanol formation was greatest at −1.1 V_{RHE} [2].

CO_2 partial pressure studies during dark electrochemistry along with Tafel analysis have previously been used to reveal the rate-determining step and reaction pathway at different metallic cathodes in aqueous electrolyte [5–22]. CO_2 partial pressure studies have also been extensively explored during photocatalytic CO_2 reduction at semiconductor electrodes, [23–25] which have a different physical response to light than plasmonically active electrodes [26]. There are some examples of studies investigating how partial pressure influences reactions at plasmonically active electrodes. Zhang et al. studied plasmon-enhanced CO_2 hydrogenation at rhodium (Rh) nanoparticles supported on titanium dioxide (TiO_2) and found differences in the thermal reaction order with H_2 partial pressure when compared to the reaction order under illuminated conditions [27]. Zhou et al. investigated ammonia (NH_3) decomposition on Cu nanoparticles on a Cu-Ru (ruthenium) surface and discovered that the plasmonic photocatalytic reaction was first-order with NH_3 pressure but the thermocatalytic reaction was zeroth-order [28]. Here we present the first report investigating how P_{CO_2} influences CO_2 reduction at a plasmonically active electrode in the dark and the light, with the goal of understanding the plasmonic mechanisms behind the light-driven selectivity and efficiency changes.

2. Experimental

2.1. Electrode preparation and characterization

The Ag electrodes were prepared and characterized as described in Creel et al. [2] Briefly, electron-beam (e-beam) evaporation was used to deposit 5 nm of titanium (Ti) on a clean glass slide followed by 200 nm of Ag. Each electrode was electrochemically conditioned for 45 min in 1.0 M potassium bicarbonate ($KHCO_3$) at −1.1 V_{RHE} before use. X-ray photoelectron spectroscopy (XPS) of the electrochemically conditioned electrodes showed only Ag, and no Ti, was present at the electrode surface.

Scanning electron microscopy (SEM) images showed nodule-like features of 10 to 100 nm. During electrochemical conditioning, these nanofeatures coarsened into larger nanostructures that were stable for hours of electrochemical experiments, as shown by UV–visible (UV–vis) absorption measurements, electrochemical surface area (ECSA) measurements, and atomic force microscopy (AFM). UV–vis results during electrochemical conditioning exhibited a plasmonic peak that broadened and red-shifted over time before reaching a steady state after 45 min with an absorption maximum at 351 nm. The ECSA decreased over time during electrochemical conditioning then stabilized after 45 min. AFM root-mean-squared (RMS) surface roughness measurements decreased from 6.0 to 4.4 nm after 45 min of electrochemical conditioning [2].

2.2. (Photo)electrochemical measurements

All (photo)electrochemical measurements were performed in the temperature-controlled photoelectrochemical cell described by Corson et al. [29] CO_2 was mixed with argon (Ar) using two mass flow controllers (Alicat, MC-10SCCM-D) to achieve the desired P_{CO_2} at a total flow rate of 5 sccm and total pressure of 1 atm (the cell was not designed for high pressure experiments). This mixture was continuously bubbled through a glass frit into the electrolyte. The electrolyte, 0.5 M potassium carbonate (K_2CO_3), was converted to 1.0 M $KHCO_3$ after saturating with CO_2 (see Table S1 for the electrolyte pH at each P_{CO_2}). The catholyte temperature was maintained at 22.0 ± 0.1°C during P_{CO_2} experiments and held at 14.0 ± 0.1°C or 32.0 ± 0.1°C at 1 atm P_{CO_2} for temperature experiments. An anion-exchange membrane (AGC Engineering Co., Ltd., Selemion AMV) separated the cathodic and anodic chambers. Platinum (Pt) foil was used as the anode. A leak-free saturated Ag/AgCl reference electrode (Innovative Instruments, Inc., LF-1) was present in the cathodic chamber. All potentials were converted to and reported versus RHE. The overpotential (η) for the CO evolution reaction was calculated using the theoretical potential ($E_T = -0.10$ V) [30] and the applied potential (E), where $\eta = E_T - E$. IR-corrected measurements were performed with a Biologic SP-300 potentiostat. Linear sweep voltammetry (LSV) measurements were performed at a rate of 5 mV s^{-1}. The Ag electrode was illuminated from the front by a 365 nm light-emitting diode (LED) (Mightex Systems, LCS-0365-48-22). The light intensity incident on the Ag electrode was 170 mW cm^{-2}, as measured by a power meter (Coherent PowerMax, PM10).

2.3. Product measurements

Gaseous products were analyzed by an in-line gas chromatograph (GC) (SRI Instruments, Multiple Gas Analyzer #5) with a 12 ft HayeSep D (divinylbenzene) column, thermal conductivity detector (TCD), and flame ionization detector (FID) preceded by a methanizer, and Ar carrier gas [29]. Chronoamperometry (CA) experiments were performed for 64 min with GC injections at 3, 15, 27, 39, 51, and 63 min. Reported current densities and FE represent the average of the last five injections. The concentration of each gas was determined using a calibration curve with points from at least three different concentrations.

Electrolyte samples from the cathodic and anodic chambers were collected at the end of each experiment and the liquid products were quantified by ^1H nuclear magnetic resonance (NMR) spectroscopy with a 500 MHz magnet (Bruker, Avance III) [30]. A water suppression method was used and concentrations in the electrolyte were determined using phenol and dimethyl sulfoxide (DMSO) as internal standards. Each product analysis experiment was performed three times on different days with a new electrode used each day. Error bars represent one standard deviation of experiments performed in triplicate.

3. Results and discussion

3.1. Total current density

LSV experiments were performed at 5 mV s^{-1} at 20, 40, 60, 80, and 100% CO_2 mol fraction (0.2 to 1 atm) in the dark and during continuous illumination at 22°C. As shown in the Tafel plots in Fig. 1 and LSV curves in Fig. S1, at a given applied overpotential, the total current increased with increasing P_{CO_2} in both the dark and the light. This trend was also observed in the dark at polycrystalline Ag in 0.1 M $KHCO_3$ [4,8]. The shift from a non-Faradaic to a Faradaic regime in the light occurred at a lower overpotential than in the dark at all P_{CO_2}. In the light the average onset potential was −0.19 V_{RHE} and in the dark the average onset potential was −0.40 V_{RHE}. Onset potentials at each P_{CO_2} in the dark and the light are tabulated in Table S2. This approximately 200 mV difference in onset potential between the light and the dark can be seen clearly by overlaying the dark and light Tafel curves at 100% CO_2 mol fraction in Fig. 2 and at all CO_2 mol fractions in Fig. S3.

There was a strong inflection point in all of the light Tafel curves at an average value of −0.3 V_{RHE} that was never observed

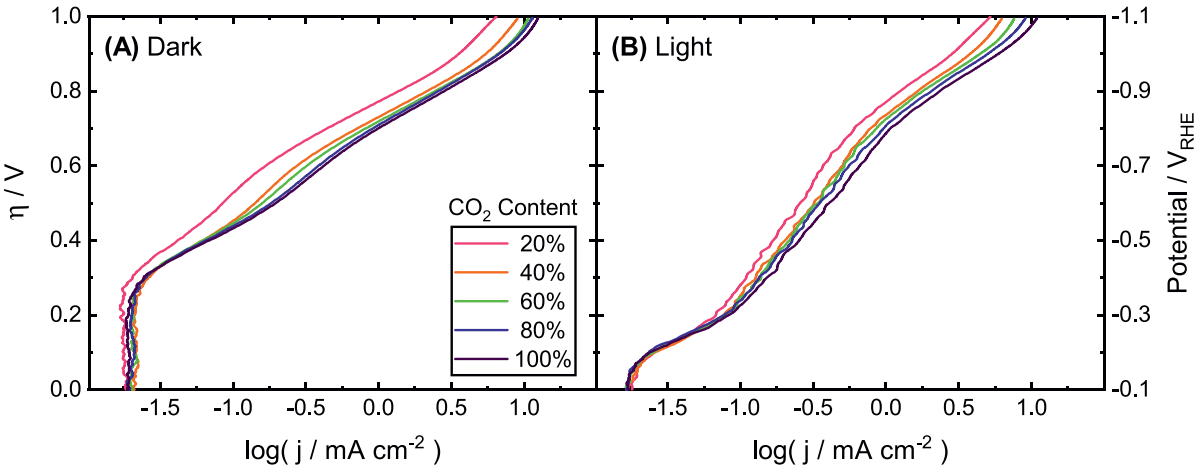

Fig. 1. Tafel plots of the total current density at various CO_2 mol fractions during linear sweep voltammetry at 5 mV s^{-1} at a silver cathode in CO_2-saturated 1.0 M $KHCO_3$ at 22°C (A) in the dark and (B) while illuminated with a 365 nm LED at 170 mW cm^{-2}. The legend in (A) applies to both (A) and (B). The overpotential (η) is shown for the CO evolution reaction. Corresponding total current density vs. potential plots are shown in Fig. S1. Overlays of light and dark Tafel plots at 100% CO_2 mol fraction are shown in Fig. 2 and at all CO_2 mol fractions are shown in Fig. S3.

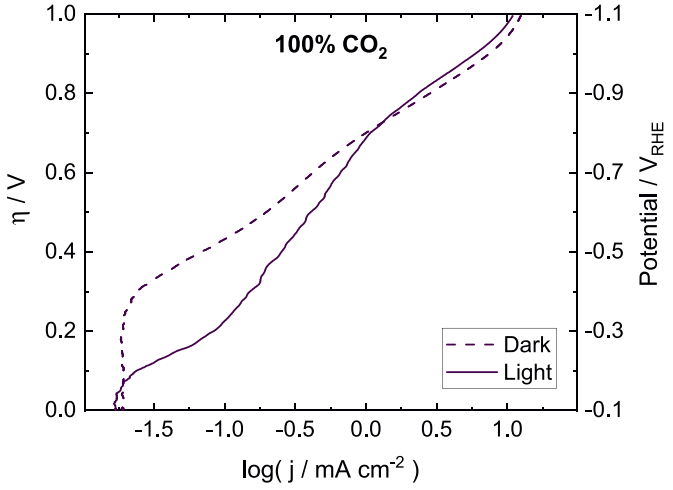

Fig. 2. Tafel plot of the total current density at 100% CO_2 mol fraction during linear sweep voltammetry at 5 mV s^{-1} at a silver cathode in CO_2-saturated 1.0 M $KHCO_3$ at 22°C in the dark (dashed line) and while illuminated with a 365 nm LED at 170 mW cm^{-2} (solid line). The overpotential (η) is shown for the CO evolution reaction. Similar overlays of light and dark Tafel plots at all CO_2 mol fractions are shown in Fig. S3. Separate light and dark Tafel plots are shown in Fig. 1 and corresponding total current density vs. potential plots are shown in Fig. S1.

in the dark. Inflection points at each P_{CO_2} in the light are tabulated in Table S2. Indeed, the total current trends in the light were different from those in the dark, especially at low overpotentials, and those trends were consistent across all P_{CO_2}. This indicates that the light does not merely shift the dark activity to a lower overpotential but fundamentally changes the electrochemical processes occurring at the cathode, as shown by changes in product selectivity in the light. For example, from previous work we know that from −0.6 to −0.8 V_{RHE} the light enhances the production of CO and suppresses H_2 evolution when compared to the dark [2]. This result is also shown in this work at −0.7 V_{RHE} for all P_{CO_2} (Figs. 3A, 4A, S4A, and S5A).

As shown in Fig. 2 and Fig. S3, the difference in dark and light activity continues from around −0.2 V_{RHE} until approximately −0.8 V_{RHE}, where the dark and light total current densities cross. The only exception to this is at 20% CO_2 mol fraction, where the dark and light curves cross at −0.88 V_{RHE}. Creel et al. found that, at potentials more negative than −0.8 V_{RHE}, there was no longer an enhancement of CO production or suppression of H_2 formation in the light when compared to the dark [2]. This shift in product distribution corresponds to the shift in the total current density trends, where the light and dark behavior at potentials more negative than −0.8 V_{RHE} are very similar, with the activity in the dark now higher than that in the light at all P_{CO_2}.

Although Figs. 1 and 2 are represented as Tafel plots, we do not use the Tafel slopes (Table S3) to identify reaction mechanisms for two key reasons. First, Dunwell et al. [31] have shown that the Tafel region for CO_2 reduction, where the overpotential is sufficiently low so that the reaction rate is kinetically controlled, occurs only at very low overpotentials (less negative than −0.4 V_{RHE}). However, in this region the product concentration is too low for reliable gaseous product quantification in our constant gas flow cell. As both H_2 and CO may form in the Tafel region in the dark we cannot reliably extract the CO partial current density.

In previous work we have shown that only CO is formed in the light at potentials less negative than −0.37 V_{RHE} [2]. Thus, we can conclude that the linear region in the light before the inflection point at −0.3 V_{RHE} is related solely to CO production. In Table S3 the Tafel slopes for CO formation in the light are calculated from −0.20 to −0.26 V_{RHE} (η = 100 to 160 mV) and range from 169 to 201 mV dec^{-1}. However, the expected Tafel slopes range from 30 to 118 mV dec^{-1} at a symmetry factor (β) of 0.5, depending on the reaction mechanism [22]. β is the fraction of the applied potential that promotes the cathodic reaction. It is only possible to achieve such high Tafel slopes if β is much lower than 0.5, indicating that only a small fraction of the total energy change is impacting the activation energy for the cathodic reaction. This brings us to our second reason for not using these Tafel slopes to identify a reaction mechanism: it is not clear that Butler-Volmer kinetics are applicable to electrochemical reactions that are influenced by a plasmonic mechanism. The Butler-Volmer equation was derived for an elementary reaction involving the transfer of a single electron from the electrode to the reactant where the energy level of the electron is defined by the applied potential.

In contrast, at an illuminated plasmonically active electrode, the excited electron energy is defined by the applied potential, the incident light wavelength, and the electronic band structure of the metal. Butler-Volmer kinetics have been applied to plasmon-enhanced electrochemical H_2 evolution at gold (Au) nanoparticles to compare Tafel slopes and exchange current densities (j_0) in

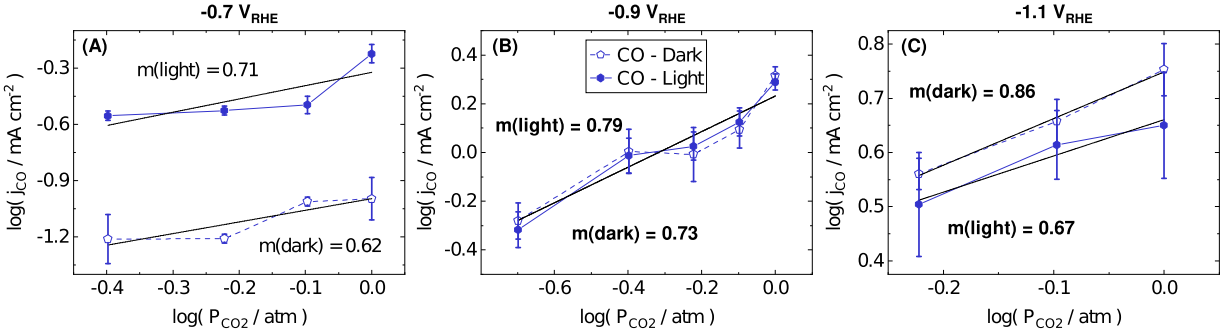

Fig. 3. Logarithm of carbon monoxide partial current density (j_{CO}) vs. logarithm of CO_2 partial pressure (P_{CO_2}) at (A) −0.7, (B) −0.9, and (C) −1.1 V_{RHE} at a silver cathode in CO_2-saturated 1.0 M $KHCO_3$ at 22°C in the dark (dashed lines) and while illuminated with a 365 nm LED at 170 mW cm^{-2} (solid lines). Error bars represent one standard deviation of experiments performed in triplicate. Black lines represent best-fit linear regression curves. Slopes in the light are shown on the graph as m(light) and slopes in the dark are shown on the graph as m(dark). Slopes in bold have R^2 values greater than 0.9. Slopes and R^2 values are also tabulated in Table S4. Corresponding Faradaic efficiencies are plotted in Fig. S4.

the dark and under illumination [32–34]. Wilson et al. proposed adding a plasmon-excitation-generated cathodic potential ($E_{h\nu}$) to the applied potential which would change j_0 but cannot account for the high Tafel slopes we observe in the light [34]. Thus, while comparing the light and dark current densities at low overpotentials is valuable for demonstrating the markedly different behavior, we cannot confidently use the Tafel slopes to identify the reaction pathway.

3.2. Carbon monoxide

Product analysis was performed at −0.7, −0.9, and −1.1 V_{RHE} at various P_{CO_2} in both dark and light conditions. At −0.9 V_{RHE} the entire range from 20% to 100% CO_2 mol fraction could be investigated, but at −0.7 and −1.1 V_{RHE} the current was unstable at lower P_{CO_2}, likely due to increased H_2 production. The product distribution at −0.7 V_{RHE} could only be investigated from 40% to 100% and −1.1 V_{RHE} was only stable from 60% to 100%.

The logarithm of the CO partial current density (j_{CO}) is plotted against the logarithm of P_{CO_2} in Fig. 3 and the FE plots are shown in Fig. S4. The slopes of the best-fit linear regression curves are shown in Fig. 3 and the slopes and R^2 values are also tabulated in Table S4. The linear regression curves in the dark and the light at −0.9 and −1.1 V_{RHE} have R^2 values greater than 0.9, indicating that the linear fit can account for greater than 90% of the variability in the data.

3.2.1. Reaction order

We expect the reaction rate, and thus j_{CO}, to depend on P_{CO_2} with some reaction order, m (Eq. 1).

$$j_{CO} \propto P_{CO_2}^{m} \tag{1}$$

By taking the logarithm of both sides we find

$$\log(j_{CO}) = m \log(P_{CO_2}) \tag{2}$$

Thus the slope of $\log(j_{CO})$ vs. $\log(P_{CO_2})$ will give the CO reaction order m with respect to P_{CO_2} (Eq. 2).

Most studies of dark CO_2 reduction on metallic cathodes find that the CO reaction is approximately first order with respect to P_{CO_2}. There are several reports of CO formation at Au cathodes at varying P_{CO_2} [5,9,14,15,18,22]. Noda et al. measured a slope of 1.2 on Au foil at −0.75 V_{RHE} in a neutral pH 0.1 M potassium phosphate (KH_2PO_4) buffer [9]. Chen et al. reported a slope of 0.92 at an oxide-derived Au cathode at −0.3 V_{RHE} in 0.5 M sodium bicarbonate ($NaHCO_3$) [14]. Wuttig et al. found slopes of 0.9 to 1.0 on polycrystalline Au films from −0.38 to −0.58 V_{RHE} in 0.1 M $NaHCO_3$ [18]. Williams et al. reported a slope of 1.2 on Au foil at −0.40 V_{RHE} in 0.1 M $NaHCO_3$ [22]. Hori et al. found slopes of 0.5 to 0.8 for CO formation on Au foil from −0.41 to −0.62 V_{RHE} in 0.5 M $KHCO_3$ [5]. Finally, Hansen et al. theoretically predicted a CO reaction order of 1 with respect to P_{CO_2} on Au(211) using a model based on density functional theory (DFT) calculations [15].

More recently there have also been reports of CO formation on Ag cathodes at varying P_{CO_2} [16,17,20,21]. A slope of 0.94 was reported for a cathode of nanoporous Ag at −0.35 V_{RHE} in 0.5 M $KHCO_3$ [16,17]. Quan et al. found a slope of 1.14 at a Ag foil at −0.90 V_{RHE} in 0.5 M $NaHCO_3$ with 20 mM of ionic liquid [20]. All of these studies concluded that CO formation at Ag cathodes has a first-order dependence on P_{CO_2}. In contrast, Singh et al. investigated a Ag foil in 0.1 M $KHCO_3$ and used a power law fit to find the intrinsic reaction order with respect to P_{CO_2} to be 1.49 at −0.9 V_{RHE}, 1.63 at −1.0 V_{RHE}, and 1.83 at −1.1 V_{RHE}, and concluded that the intrinsic reaction order is greater than one [21]. We note that the slopes closest to one on both Au and Ag cathodes were performed at low overpotentials where mass transfer effects are minimal, ca. −0.35 V_{RHE} [14,16–18].

In this study of Ag cathodes we find the average value of slopes in the dark and light are statistically similar and roughly 0.7 at all potentials studied (Fig. 3), although in the dark a slight increase in slope is observed with increasing overpotential (from 0.62 at −0.7 V_{RHE} to 0.86 at −1.1 V_{RHE}). From this we conclude that the reaction order of CO with respect to P_{CO_2} is likely first order in both the dark and the light; the experimentally measured slopes may be less than one due to the influence of mass transfer limitations [21].

The possible reaction mechanisms for CO formation and their reaction order with P_{CO_2} are nicely summarized by Williams et al. [22]. The majority are first order with P_{CO_2}, but some reaction mechanisms would result in second order behavior. From our results in Fig. 3 we can conclude that the light does not cause the reaction mechanism to change from a mechanism that is first order with P_{CO_2} to one that is second order with P_{CO_2}. We can also state that the reaction order of CO with respect to P_{CO_2} is first order in both the dark and the light, likely indicating that the rate-determining step does not change upon illumination. This is consistent with the conclusion from the attenuated total reflectance surface-enhanced infrared absorption spectroscopy (ATR–SEIRAS) report that light enhanced the CO desorption from the Ag surface rather than influencing the reaction pathway [35]. However, this data alone cannot conclusively identify the reaction pathway nor discount that the reaction mechanism in the light may be a different first-order pathway than that in the dark.

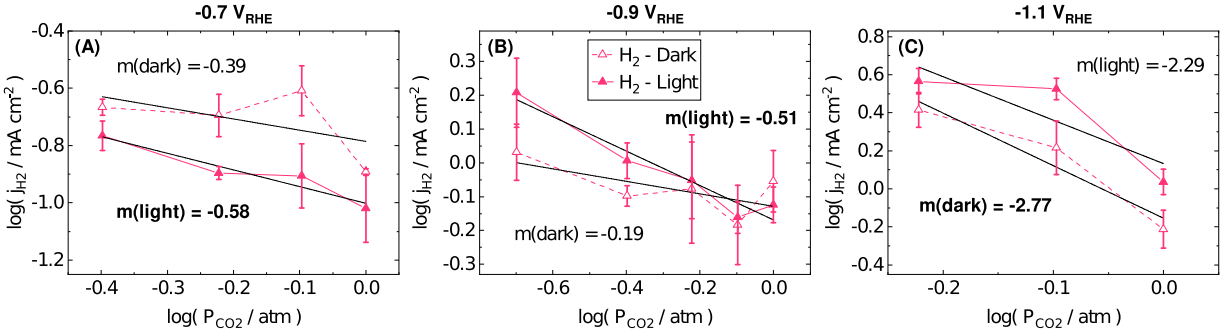

Fig. 4. Logarithm of hydrogen partial current density (j_{H_2}) vs. logarithm of CO_2 partial pressure (P_{CO_2}) at (A) −0.7, (B) −0.9, and (C) −1.1 V_{RHE} at a silver cathode in CO_2-saturated 1.0 M $KHCO_3$ at 22°C in the dark (dashed lines) and while illuminated with a 365 nm LED at 170 mW cm^{-2} (solid lines). Error bars represent one standard deviation of experiments performed in triplicate. Black lines represent best-fit linear regression curves. Slopes in the light are shown on the graph as m(light) and slopes in the dark are shown on the graph as m(dark). Slopes in bold have R^2 values greater than 0.9. Slopes and R^2 values are also tabulated in Table S4. Corresponding Faradaic efficiencies are plotted in Fig. S5.

3.2.2. Reaction order trends with applied potential

As mentioned earlier, we find that the slope in the dark increases slightly with more negative applied potentials: 0.62 at −0.7 V_{RHE}, 0.73 at −0.9 V_{RHE}, and 0.86 at −1.1 V_{RHE}. However, this trend is broken in the light with a smaller slope at −1.1 V_{RHE} than at −0.7 or −0.9 V_{RHE}. The same trend of increasing reaction order with more negative potentials was reported in the study by Singh et al from −0.9 to −1.1 V_{RHE}. They concluded that the reaction order increases because the adsorption free energy of CO_2 on Ag increases with more negative potentials due to stronger π back-bonding [21].

It is possible for the local electric fields that can be generated at an illuminated plasmonically active cathode to influence the adsorption energy of species, which could account for the different slope trend in the light. However, an ATR–SEIRAS study showed no shift in the peak position of adsorbed CO_2 upon illumination (365 nm LED, 125 mW cm^{-2}) of a plasmonically active Ag cathode during CO_2 reduction in 0.1 M $KHCO_3$ at −0.6 or −0.7 V_{RHE}. The CO_2 peak position additionally did not shift in the dark with potential from −0.7 to −0.9 V_{RHE}, [35] even though the postulated stronger π back-bonding should cause the wavenumber to increase with more negative potentials.

No other Ag study has reported P_{CO_2} at more than one applied potential. Of the reports on Au that explored multiple applied potentials, neither Hori et al. nor Wuttig et al. observed the reaction order increasing with greater overpotentials [5,18]. Nevertheless, given the statistical similarity in the P_{CO_2} reaction orders among all measurements described in Fig. 3, at this time there is not enough evidence on Ag to conclude whether or not the dark reaction order with P_{CO_2} truly increases with more negative potentials and if there is a change in this trend upon illumination.

3.3. Hydrogen

The logarithm of the H_2 partial current density (j_{H_2}) is plotted against the logarithm of P_{CO_2} in Fig. 4 and the FE plots are shown in Fig. S4. The slopes of the best-fit linear regression curves are shown in Fig. 4 and the slopes and R^2 values are also tabulated in Table S4. Only half of the linear regression curves have R^2 values greater than 0.9, indicating that the log of j_{H_2} is only approximately linear with the logarithm of P_{CO_2} in both the dark and the light.

As CO_2 does not participate in the H_2 evolution reaction, the reaction rate expression does not depend on P_{CO_2}. However, we find that j_{H_2} decreases with increasing P_{CO_2} at all applied potentials in both the dark and the light. This trend has also been theoretically predicted [12] and experimentally observed on Cu [6,7] and indium (In) [10]. While one study on Cu was also performed at CO_2 pressures at and below 1 atm, [6] the second report on Cu [7] and the study on In [10] investigated CO_2 pressures of 1 to 60 atm and both found H_2 production continued to decrease throughout this range.

This decrease in H_2 evolution with increasing P_{CO_2} in both the dark and the light indicates a competition in adsorption between the H_2 and CO reactants, as shown in Fig. 5. Indeed, j_{H_2} decreases and j_{CO} increases with increasing P_{CO_2} at all applied potentials with and without illumination. Chaplin et al. predicted that increasing P_{CO_2} would promote the retention of CO_x^{y-} species and suppress H(ads) coverage [12]. At illuminated plasmonically active electrodes it is possible for local electric fields or hot electrons to influence the binding energy, and thus coverage, of adsorbates. While there are differences in the H_2 slopes with P_{CO_2} between the light and the dark at each applied potential (Fig. 4), the difference is not sufficiently significant to determine if the light is affecting the CO_x^{y-} or H(ads) adsorbate coverage on this cathode.

3.4. Liquid products

In agreement with our previous study, [2] there were two liquid products formed in this investigation, formate and methanol. The logarithm of the formate partial current density (j_{HCOO^-}) is plotted against the logarithm of P_{CO_2} in Fig. 6 and the FE plots are shown in Fig. S6. The slopes and $R1^2$ values of the best-fit linear regression curves are tabulated in Table S4. All of the linear regression curves have R^2 values much lower than 0.9, indicating that the linear fit cannot account for most of the variability in the data.

As the slopes and R^2 values are quite low, it appears that the production of formate has very little dependence on P_{CO_2} in the pressure range of 0.2 to 1 atm at this Ag cathode. When studying much higher P_{CO_2}, Hara et al. found that the formate FE increased from 0.8% at 1 atm to 17% at 30 atm at a Ag wire in 0.1 M $KHCO_3$ at −0.9 V_{RHE} [8]. Todoroki also found that formate formation increased with P_{CO_2} from 1 to 60 atm at an In electrode in 0.5 M $KHCO_3$ under galvanostatic conditions, reaching nearly 100% FE by 20 atm [10]. Kyriacou et al. found that the formate FE increased from 5% to 20% with P_{CO_2} from 0.15 to 1 atm over a Cu foil electrode in 0.5 M $KHCO_3$ at −1.0 V_{RHE} [6] and Hara et al. similarly found that the formate FE increased from 0.8% to 13.7% from 10 to 60 atm over a Cu wire electrode in 0.1 M $KHCO_3$ at −1.0 V_{RHE} [7]. Chaplin et al. reviewed and tabulated experimental results of CO_2 reduction at 25 different metallic electrodes, summarizing that high CO_2 pressure especially favors formate production and suppresses H_2 evolution at *sp* metals (metals whose valence electrons are in the

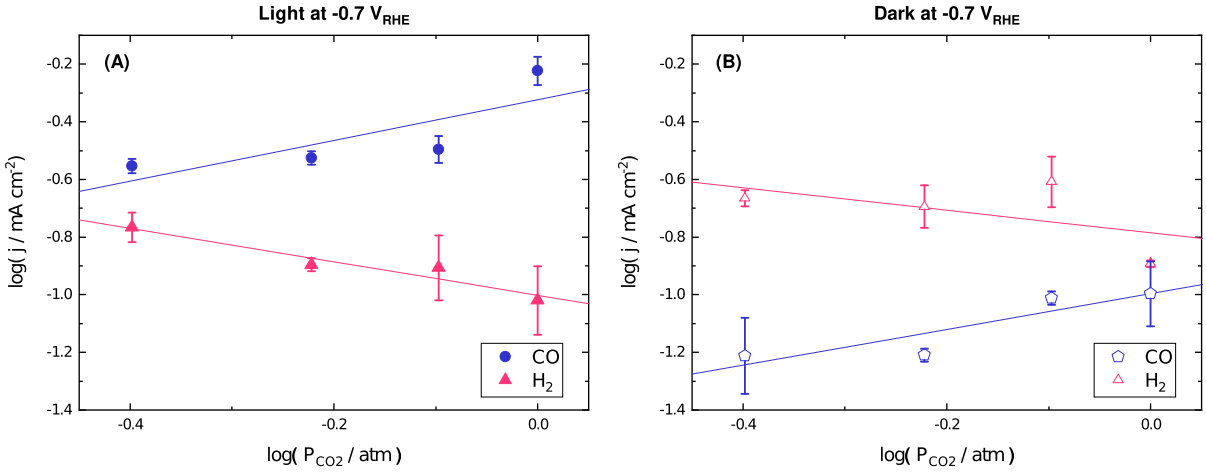

Fig. 5. Logarithm of carbon monoxide and hydrogen partial current densities (j) vs. logarithm of CO_2 partial pressure (P_{CO_2}) at −0.7 V_{RHE} at a silver cathode in CO_2-saturated 1.0 M $KHCO_3$ at 22°C (A) while illuminated with a 365 nm LED at 170 mW cm^{-2} and (B) in the dark. Error bars represent one standard deviation of experiments performed in triplicate. Lines represent best-fit linear regression curves. Slopes and R^2 values are tabulated in Table S4. Partial current densities at other potentials in the dark and the light are plotted in Figs. 3 and 4 and corresponding Faradaic efficiencies are plotted in Figs. S4 and S5.

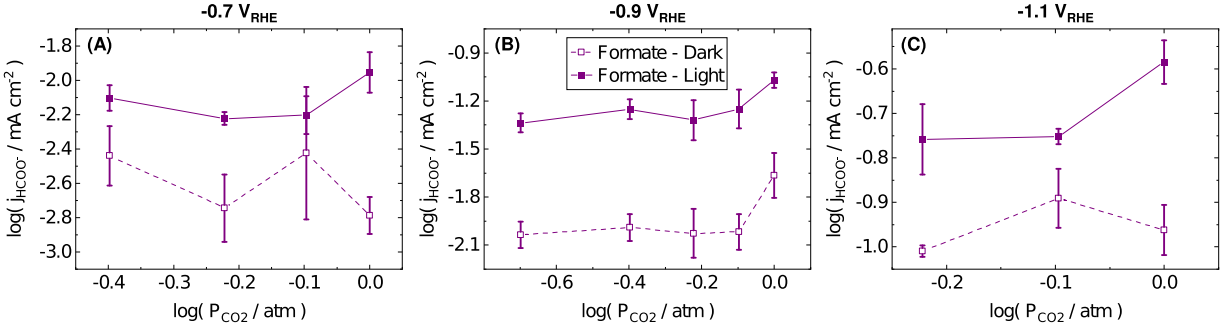

Fig. 6. Logarithm of formate partial current density (j_{HCOO^-}) vs. logarithm of CO_2 partial pressure (P_{CO_2}) at (A) −0.7, (B) −0.9, and (C) −1.1 V_{RHE} at a silver cathode in CO_2-saturated 1.0 M $KHCO_3$ at 22°C in the dark (dashed lines) and while illuminated with a 365 nm LED at 170 mW cm^{-2} (solid lines). Slopes and R^2 values are tabulated in Table S4. All R^2 values are much lower than 0.9. Corresponding Faradaic efficiencies are plotted in Fig. S6.

sp orbitals) such as In or tin (Sn) [12]. It appears that a formate dependence on P_{CO_2} is observed only at much higher pressures for cathodes with low selectivity towards formate, or at pressures less than 1 atm for catalysts with higher selectivity.

There is no significant difference between the formate trends in the dark and the light at any applied potential; both exhibit what is statistically a zeroth order dependence on P_{CO_2}, which is likely not the true reaction order. Of the proposed mechanisms for CO_2 reduction to formate, most would result in a reaction order of one with respect to P_{CO_2} [36–38] with one proposed mechanism resulting in second order dependence [39]. In some reaction pathways, CO and formate share the same reaction intermediate [36,38] and in others the pathways are completely distinct, [37–39] but both CO and formate are competing for CO_2. As CO production changes significantly with P_{CO_2} and has partial current densities 1 to 2 orders of magnitude larger than those of formate, it may obscure the actual dependence of formate on P_{CO_2}.

The second liquid product, methanol, was only detected in the light at −0.9 and −1.1 V_{RHE}. The logarithm of the methanol partial current density (j_{CH_3OH}), is plotted against the logarithm of P_{CO_2} in Fig. 7 and the FE plots are shown in Fig. S7. The slopes and R^2 values of the best-fit linear regression curves are tabulated in Table S4. The two linear regression curves have R^2 values much lower than 0.9, indicating that the linear fit cannot account for most of the variability in the data.

There are no prior studies of CO_2 reduction at metal electrodes in aqueous electrolyte that explore the dependence of methanol formation on P_{CO_2}. Lais et al. reviewed the research on the photoreduction of CO_2 at TiO_2 and found that methanol formation beginning at 1 atm initially increased with increasing P_{CO_2}, reached an optimal pressure for peak methanol formation (1.2, 1.3, or 10 atm), then decreased at higher pressures [25]. Li et al. studied methanol formation at a Cu disk in an ethanol-water solution of 0.1 M lithium chloride and found that the current increased with increasing P_{CO_2} from 14 to 54 atm and was independent of P_{CO_2} up to 95 atm [11]. In the pyridine-catalyzed reduction of CO_2 to methanol at a Pt foil in 0.5 M potassium chloride (KCl) both Morris et al. and Rybchenko et al. found that the current increased with increasing P_{CO_2} (1 to 6 atm and 1 to 50 atm, respectively) [13,19]. While Morris et al. concluded that the rate-determining step for methanol formation was first order with P_{CO_2}, [13] Rybchenko et al. determined that the increase in current was not related to methanol formation [19].

In this study we find no significant dependence of methanol formation in the light with 0.2 to 1 atm P_{CO_2}. This difference from the previous studies may be due to the lower pressure or because the cathode material and operating conditions are significantly different. While the exact mechanism of CO_2 reduction to methanol on Ag is unknown, the reaction pathway is thought to involve either CO or formate as an intermediate [40]. As there are variations in both CO and formate production with P_{CO_2} in the light at −0.9 and −1.1 V_{RHE} and j_{CH_3OH} is one order of magnitude lower than j_{HCOO^-} and two orders of magnitude lower than j_{CO}, the true dependence of methanol production on P_{CO_2} may be masked.

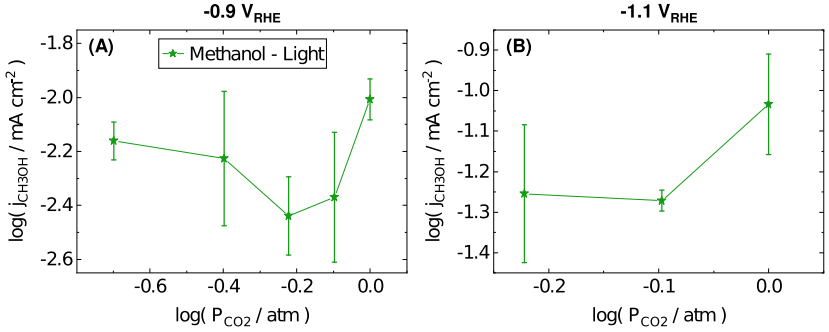

Fig. 7. Logarithm of methanol partial current density (j_{CH_3OH}) vs. logarithm of CO_2 partial pressure (P_{CO_2}) at (A) −0.9 and (B) −1.1 V_{RHE} at a silver cathode in CO_2-saturated 1.0 M $KHCO_3$ at 22°C while illuminated with a 365 nm LED at 170 mW cm^{-2}. No methanol was measured in the dark at any applied potential and no methanol was measured under illuminated conditions at −0.7 V_{RHE}. Slopes and R^2 values are tabulated in Table S4. All R^2 values are less than 0.9. Corresponding Faradaic efficiencies are plotted in Fig. S7.

3.5. Temperature

Product variations with temperature were studied at 14, 22, and 32°C at 1 atm P_{CO_2} in the dark and the light at −0.7, −0.9, and −1.1 V_{RHE}. Partial current density variations with temperature and applied potential are shown for CO (Fig. S8), H_2 (Fig. S9), formate (Fig. S10), and methanol (Fig. S11). These plots correspond with the FE plots for CO (Fig. S12), H_2 (Fig. S13), formate (Fig. S14), and methanol (Fig. S15).

Overall, very little variation was observed between 14 and 22°C for all products, likely reflecting the opposing influences of a decrease in reaction rate with an increase in CO_2 solubility at 14°C. From 22 to 32°C the general trend was a decrease in CO_2 reduction product formation and an increase in H_2 evolution. This cannot solely be explained by a decrease in CO_2 solubility at 32°C because the selectivity does not match that at 0.8 atm P_{CO_2} where the CO_2 concentration is expected to be similar (Fig. S16). While there are some differences in temperature trends between the dark and the light, they are difficult to interpret in terms of reaction kinetics due to the changes in selectivity caused by the light and differences in CO_2 concentration.

However, these findings provide additional support to our prior claim that plasmon-driven selectivity changes at an illuminated Ag cathode were not due to local heating, [2] which can occur when plasmonic electronic excitations thermalize [41]. Where CO production was enhanced and H_2 evolution was suppressed in the light when compared to the dark from −0.6 to −0.8 V_{RHE}, [2] here we show at −0.7 V_{RHE} that an increase in temperature causes a decrease in CO formation (Fig. S12) and an increase in H_2 production (Fig. S13). While formate was enhanced in the light at most potentials with a maximum difference at −0.9 V_{RHE}, [2] here we see that formate decreases at elevated temperatures at −0.9 V_{RHE} (Fig. S14). Finally, where methanol is only produced in the light beginning at −0.8 V_{RHE}, [2] we find that an increase in temperature causes methanol production to decrease at both −0.9 and −1.1 V_{RHE} (Fig. S15).

4. Conclusions

Our measurements of the CO_2 reduction activity and product distribution trends at a plasmonically active Ag cathode across a range of P_{CO_2} (0.2 to 1 atm) and temperatures (14 to 32°C) at multiple applied potentials (−0.7, −0.9, and −1.1 V_{RHE}) can be used to understand the light-driven selectivity changes. We observed that the total current density increased with increasing P_{CO_2} in both the dark and the light. However, the Tafel curves were significantly different between dark and illuminated conditions, showing that the light does not merely shift the dark activity to lower overpotentials but changes the selectivity. Furthermore, we found that the CO activity at very low overpotentials in the light likely cannot be modeled by a Tafel equation, indicating that Butler-Volmer kinetics may not apply to plasmon-enhanced electrochemical reactions.

Examining the product distribution trends, we found that the CO reaction order with P_{CO_2} was first order in both the dark and the light, likely indicating that the rate-determining step is not changed upon illumination. We showed that H_2 evolution decreased with P_{CO_2} at slightly different rates with and without illumination, making it unclear if a plasmonic mechanism was influencing the CO or H_2 intermediate adsorbate coverage. While formate and methanol formation were both zeroth order with P_{CO_2} in the dark and the light, the relatively low activity of these two products with respect to CO and H_2 production may mask the true reaction orders. As in other studies, it may be possible to measure more accurate formate and methanol reaction orders at much higher pressures outside of our experimental capabilities.

Finally, we observed that increasing the electrolyte temperature decreased the selectivity for CO_2 reduction products and increased the formation of H_2. As these trends are exactly the opposite of what we observe upon illumination, we conclude that the plasmon-induced selectivity changes are not caused by local heating of the cathode surface. Future studies using time-resolved in situ spectroscopy techniques that can detect reaction intermediates, such as surface-enhanced Raman spectroscopy (SERS) or surface-enhanced infrared absorption spectroscopy (SEIRAS), could resolve the unknown plasmonic mechanisms. New electrodes with nanostructured surfaces that enhance the spectroscopic signal will increase the likelihood of detecting reaction intermediates. While we continue to search for the plasmonic mechanisms that drive the enhancement of CO_2 reduction to CO, formate, and methanol while suppressing H_2 evolution at an illuminated Ag cathode, this study has helped to eliminate several possible pathways.

Declaration of competing interest

The authors declare that they have no known competing financial interests or personal relationships that could have appeared to influence the work reported in this paper.

Credit authorship contribution statement

Elizabeth R. Corson: Investigation, Formal analysis, Writing - original draft, Writing - review & editing. **Erin B. Creel:** Investigation, Writing - review & editing. **Robert Kostecki:** Writing - review & editing, Funding acquisition. **Jeffrey J. Urban:** Writing - review & editing, Funding acquisition. **Bryan D. McCloskey:** Writing - review & editing, Funding acquisition.

Acknowledgments

This work was supported by the National Science Foundation (CBET-1653430); the Joint Center for Artificial Photosynthesis, a DOE Energy Innovation Hub, supported through the Office of Science of the U.S. Department of Energy (DE-SC0004993); the Molecular Foundry, supported through the Office of Science, Office of Basic Energy Sciences of the U.S. Department of Energy (DE-AC02-05CH11231); and the National Science Foundation Graduate Research Fellowship (DGE 1106400).

Supplementary material

Supplementary material associated with this article can be found, in the online version, at 10.1016/j.electacta.2021.137820.

References

[1] Y. Kim, E.B. Creel, E.R. Corson, B.D. McCloskey, J.J. Urban, R. Kostecki, Surface-plasmon-assisted photoelectrochemical reduction of CO_2 and NO_3^- on nanostructured silver electrodes, Adv. Energy Mater. 8 (2018) 1800363, doi:10.1002/aenm.201800363.

[2] E.B. Creel, E.R. Corson, J. Eichhorn, R. Kostecki, J.J. Urban, B.D. McCloskey, Directing selectivity of electrochemical carbon dioxide reduction using plasmonics, ACS Energy Lett. 4 (2019) 1098–1105, doi:10.1021/acsenergylett.9b00515.

[3] E.R. Corson, S. Subramani, J.K. Cooper, R. Kostecki, J.J. Urban, B.D. McCloskey, Reduction of carbon dioxide at a plasmonically active copper-silver cathode, Chem. Commun. 56 (2020) 9970–9973, doi:10.1039/d0cc03215h.

[4] T. Hatsukade, K.P. Kuhl, E.R. Cave, D.N. Abram, T.F. Jaramillo, Insights into the electrocatalytic reduction of CO_2 on metallic silver surfaces, Phys. Chem. Chem. Phys. 16 (27) (2014) 13814–13819, doi:10.1039/c4cp00692e.

[5] Y. Hori, A. Murata, K. Kikuchi, S. Suzuki, Electrochemical reduction of carbon dioxide to carbon monoxide at a gold electrode in aqueous potassium hydrogen carbonate, J. Chem. Soc. (1987) 728–729, doi:10.1039/C39870000728.

[6] G.Z. Kyriacou, A.K. Anagnostopoulos, Influence of CO_2 partial pressure and the supporting electrolyte cation on the product distribution in CO_2 electroreduction, J. Appl. Electrochem. 23 (1993) 483–486.

[7] K. Hara, A. Tsuneto, A. Kudo, T. Sakata, Electrochemical reduction of CO_2 on a Cu electrode under high pressure: factors that determine the product selectivity, J. Electrochem. Soc. 141 (1994) 2097–2103.

[8] K. Hara, A. Kudo, T. Sakata, Electrochemical reduction of carbon dioxide under high pressure on various electrodes in an aqueous electrolyte, J. Electroanal. Chem. 391 (1995) 141–147, doi:10.1016/0022-0728(95)03935-A.

[9] H. Noda, S. Ikeda, A. Yamamoto, H. Einaga, K. Ito, Kinetics of electrochemical reduction of carbon dioxide on a gold electrode in phosphate buffer solutions, Bull. Chem. Soc. Jpn. 68 (1995) 1889–1895, doi:10.1246/bcsj.68.1889.

[10] M. Todoroki, K. Hara, A. Kudo, T. Sakata, Electrochemical reduction of high pressure CO_2 at Pb, Hg and In electrodes in an aqueous $KHCO_3$ solution, J. Electroanal. Chem. 394 (1995) 199–203, doi:10.1016/0022-0728(95)04010-L.

[11] J. Li, G. Prentice, Electrochemical synthesis of methanol from CO_2 in high-pressure electrolyte, J. Electrochem. Soc. 144 (1997) 4284–4288, doi:10.1149/1.1838179.

[12] R. Chaplin, A. Wragg, Effects of process conditions and electrode material on reaction pathways for carbon dioxide electroreduction with particular reference to formate formation, J. Appl. Electrochem. 33 (2003) 1107–1123, doi:10.1023/B:JACH.0000004018.57792.b8.

[13] A.J. Morris, R.T. McGibbon, A.B. Bocarsly, Electrocatalytic carbon dioxide activation: the rate-determining step of pyridinium-catalyzed CO_2 reduction, ChemSusChem 4 (2) (2011) 191–196, doi:10.1002/cssc.201000379.

[14] Y. Chen, C.W. Li, M.W. Kanan, Aqueous CO_2 reduction at very low overpotential on oxide-derived Au nanoparticles, J. Am. Chem. Soc. 134 (49) (2012) 19969–19972, doi:10.1021/ja309317u.

[15] H.A. Hansen, J.B. Varley, A.A. Peterson, J.K. Norskov, Understanding trends in the electrocatalytic activity of metals and enzymes for CO_2 reduction to CO, J. Phys. Chem. Lett. 4 (3) (2013) 388–392, doi:10.1021/jz3021155.

[16] Q. Lu, J. Rosen, Y. Zhou, G.S. Hutchings, Y.C. Kimmel, J.G. Chen, F. Jiao, A selective and efficient electrocatalyst for carbon dioxide reduction, Nat. Commun. 5 (2014) 3242, doi:10.1038/ncomms4242.

[17] J. Rosen, G.S. Hutchings, Q. Lu, S. Rivera, Y. Zhou, D.G. Vlachos, F. Jiao, Mechanistic insights into the electrochemical reduction of CO_2 to CO on nanostructured Ag surfaces, ACS Catal. 5 (7) (2015) 4293–4299, doi:10.1021/acscatal.5b00840.

[18] A. Wuttig, M. Yaguchi, K. Motobayashi, M. Osawa, Y. Surendranath, Inhibited proton transfer enhances Au-catalyzed CO_2-to-fuels selectivity, Proc. Natl. Acad. Sci. USA 113 (32) (2016) E4585–93, doi:10.1073/pnas.1602984113.

[19] S.I. Rybchenko, D. Touhami, J.D. Wadhawan, S.K. Haywood, Study of pyridine-mediated electrochemical reduction of CO_2 to methanol at high CO_2 pressure, ChemSusChem 9 (13) (2016) 1660–1669, doi:10.1002/cssc.201600267.

[20] F. Quan, M. Xiong, F. Jia, L. Zhang, Efficient electroreduction of CO_2 on bulk silver electrode in aqueous solution via the inhibition of hydrogen evolution, Appl. Surf. Sci. 399 (2017) 48–54, doi:10.1016/j.apsusc.2016.12.069.

[21] M.R. Singh, J.D. Goodpaster, A.Z. Weber, M. Head-Gordon, A.T. Bell, Mechanistic insights into electrochemical reduction of CO_2 over Ag using density functional theory and transport models, Proc. Natl. Acad. Sci. USA 114 (42) (2017) E8812–E8821, doi:10.1073/pnas.1713164114.

[22] K. Williams, N. Corbin, J. Zeng, N. Lazouski, D.-T. Yang, K. Manthiram, Protecting effect of mass transport during electrochemical reduction of oxygenated carbon dioxide feedstocks, Sustain. Energy Fuels 3 (5) (2019) 1225–1232, doi:10.1039/c9se00024k.

[23] B. Kumar, M. Llorente, J. Froehlich, T. Dang, A. Sathrum, C.P. Kubiak, Photochemical and photoelectrochemical reduction of CO_2, Annu. Rev. Phys. Chem. 63 (2012) 541–569, doi:10.1146/annurev-physchem-032511-143759.

[24] N. Shehzad, M. Tahir, K. Johari, T. Murugesan, M. Hussain, A critical review on TiO_2 based photocatalytic CO_2 reduction system: strategies to improve efficiency, J. CO_2 Util. 26 (2018) 98–122, doi:10.1016/j.jcou.2018.04.026.

[25] A. Lais, M.A. Gondal, M.A. Dastageer, F.F. Al-Adel, Experimental parameters affecting the photocatalytic reduction performance of CO_2 to methanol: a review, Int. J. Energy Res. 42 (6) (2018) 2031–2049, doi:10.1002/er.3965.

[26] E.R. Corson, E.B. Creel, R. Kostecki, B.D. McCloskey, J.J. Urban, Important considerations in plasmon-enhanced electrochemical conversion at voltage-biased electrodes, iScience 23 (3) (2020) 100911, doi:10.1016/j.isci.2020.100911.

[27] X. Zhang, X. Li, M.E. Reish, D. Zhang, N.Q. Su, Y. Gutierrez, F. Moreno, W. Yang, H.O. Everitt, J. Liu, Plasmon-enhanced catalysis: distinguishing thermal and nonthermal effects, Nano Lett. 18 (3) (2018) 1714–1723, doi:10.1021/acs.nanolett.7b04776.

[28] L. Zhou, D.F. Swearer, C. Zhang, H. Robatjazi, H. Zhao, L. Henderson, L. Dong, P. Christopher, E.A. Carter, P. Nordlander, N.J. Halas, Quantifying hot carrier and thermal contributions in plasmonic photocatalysis, Science 362 (2018) 60–72, doi:10.1126/science.aat6967.

[29] E.R. Corson, E.B. Creel, Y. Kim, J.J. Urban, R. Kostecki, B.D. McCloskey, A temperature-controlled photoelectrochemical cell for quantitative product analysis, Rev. Sci. Instrum. 89 (5) (2018) 055112, doi:10.1063/1.5024802.

[30] K.P. Kuhl, E.R. Cave, D.N. Abram, T.F. Jaramillo, New insights into the electrochemical reduction of carbon dioxide on metallic copper surfaces, Energy Environ. Sci. 5 (2012) 7050–7059, doi:10.1039/c2ee21234j.

[31] M. Dunwell, W. Luc, Y. Yan, F. Jiao, B. Xu, Understanding surface-mediated electrochemical reactions: CO_2 reduction and beyond, ACS Catal. 8 (9) (2018) 8121–8129, doi:10.1021/acscatal.8b02181.

[32] X. Guo, X. Li, S. Kou, X. Yang, X. Hu, D. Ling, J. Yang, Plasmon-enhanced electrocatalytic hydrogen/oxygen evolution by Pt/Fe-Au nanorods, J. Mater. Chem. A 6 (17) (2018) 7364–7369, doi:10.1039/c8ta00499d.

[33] H.X. Zhang, Y. Li, M.Y. Li, H. Zhang, J. Zhang, Boosting electrocatalytic hydrogen evolution by plasmon-driven hot-electron excitation, Nanoscale 10 (5) (2018) 2236–2241, doi:10.1039/c7nr08474a.

[34] A.J. Wilson, V. Mohan, P.K. Jain, Mechanistic understanding of plasmon-enhanced electrochemistry, J. Phys. Chem. C 123 (48) (2019) 29360–29369, doi:10.1021/acs.jpcc.9b10473.

[35] E.R. Corson, R. Kas, R. Kostecki, J.J. Urban, W.A. Smith, B.D. McCloskey, R. Kortlever, In situ ATR–SEIRAS of carbon dioxide reduction at a plasmonic silver cathode, J. Am. Chem. Soc. 142 (2020) 11750–11762, doi:10.1021/jacs.0c01953.

[36] A.A. Peterson, F. Abild-Pedersen, F. Studt, J. Rossmeisl, J.K. Norskov, How copper catalyzes the electroreduction of carbon dioxide into hydrocarbon fuels, Energy Environ. Sci. 3 (2010) 1311–1315, doi:10.1039/c0ee00071j.

[37] T. Cheng, H. Xiao, W.A. Goddard, Reaction mechanisms for the electrochemical reduction of CO_2 to CO and formate on the Cu(100) surface at 298 K from quantum mechanics free energy calculations with explicit water, J. Am. Chem. Soc. 138 (42) (2016) 13802–13805, doi:10.1021/jacs.6b08534.

[38] C.W. Lee, N.H. Cho, K.D. Yang, K.T. Nam, Reaction mechanisms of the electrochemical conversion of carbon dioxide to formic acid on tin oxide electrodes, ChemElectroChem 4 (9) (2017) 2130–2136, doi:10.1002/celc.201700335.

[39] A. Gennaro, A.A. Isse, M. Severin, E. Vianello, I. Bhugun, J. Saveant, Mechanism of the electrochemical reduction of carbon dioxide at inert electrodes in media of low proton availability, J. Chem. Soc. Faraday Trans. 92 (20) (1996) 3963–3968, doi:10.1039/FT9969203963.

[40] J. Albo, M. Alvarez-Guerra, P. Castaño, A. Irabien, Towards the electrochemical conversion of carbon dioxide into methanol, Green Chem. 17 (4) (2015) 2304–2324, doi:10.1039/c4gc02453b.

[41] S. Linic, U. Aslam, C. Boerigter, M. Morabito, Photochemical transformations on plasmonic metal nanoparticles, Nat. Mater. 14 (6) (2015) 567–576, doi:10.1038/nmat4281.